Journal of Applied Polymer Science

Crystalline Phase Transformation of Polytetrafluoroethylene in a Fatigue Test

S. B. Yang,[1] X. X. Pu,[2] Z. Y. Huang,[1] Q. Y. Wang[1,3]

[1]Key Laboratory of Energy Engineering Safety and Disaster Mechanics, Ministry of Education, Sichuan University, Chengdu 610065 China

[2]Polymer Research Institute, Sichuan University, Chengdu 610065 China

[3]Chengdu University, Chengdu 610106 China

Correspondence to: Q. Y. Wang (E-mail: wangqy@scu.edu.cn)

In this study, we aimed to characterize the mechanical response of polytetrafluoroethylene (PTFE) laminates under a tension–tension load-control fatigue test (frequency = 5 Hz, load ratio = 0) and provided an analysis of the failure patterns of the PTFE material with consideration of crystalline phase transformation. In the final results, the evolution of the cyclic creep strain and stress–number of cycles to failure (S–N) curves presented duplex properties accompanying the fatigue life increasing to high cycles (cycle fatigue $> 10^5$). A simple phenomenological damage index was defined in this study to describe the cyclic creep process. Additionally, the scanning electronic machine investigation suggested that local fibrosis caused by crystalline phase transformation to phase I led to the initiation of fatigue crack, and the fiber formation and orientation was found to be beneficial to a higher tensile strength and better resistance to crack propagation. The aspect of cyclic-load-induced crystallization was observed by the microfocus hard X-ray diffraction beamline from a new insight. The crystalline phase transformation led to a gradient distribution of crystallinity and lateral crystallite size along the crack propagation direction. © 2014 Wiley Periodicals, Inc. J. Appl. Polym. Sci. **2014**, *131*, 41113.

KEYWORDS: biomaterials; microscopy; phase behavior; properties and characterization; thermoplastics

Received 21 April 2014; accepted 3 June 2014

DOI: 10.1002/app.41113

INTRODUCTION

Polytetrafluoroethylene (PTFE), a semicrystalline polymer, has been used in a wide range of engineering applications. It notably serves as biological implants, ranging from single-component PTFE structures to sliding contact pads in complex joints, because of its extremely low coefficient of friction, resistance to corrosion, better mechanical properties, and superior biocompatibility.[1–5] These substitutes are required to work for extensive periods under cyclic loading conditions.[6] Hence, it is necessary to understand its fatigue performance and behavior.

Failure mechanisms of PTFE have been investigated in studies,[7–9] but the fatigue failure and behavior cannot be completely understood, as has been found in general for thermoplastic materials. The effects of the processing variables on the fatigue in unfilled and short fiber-reinforced PTFEs with notching pretreatment have been discussed by several research groups,[10–13] and fatigue crack propagation (FCP) aspects have mainly been considered. Fatigue crack resistance has shown a complex interdependence of various factors, including the molecular weight, crystallinity and fiber variety, dosage of the filler, loading frequency and stress level, and environmental temperature. FCP has also been correlated to the microstructure by means of a microstructural efficiency parameter related to the layered fiber distribution observed in short-fiber-reinforced thermoplastics.[14] However, there have been few studies investigating on the fatigue crack initiation (FCI) aspects of PTFE, which present a significant influence on the FCP patterns. The inert nature of PTFE allows the crystalline phase to transform with changes in the temperature. The crystalline structure of pure PTFE exhibits two atmospheric pressure crystalline transitions at 19°C from the triclinic structure (phase II) to a partially ordered hexagonal structure (phase IV) and at 30°C to the pseudohexagonal structure (phase I).[15] Meanwhile, the fracture behavior of PTFE undergoes transitions from brittle fracture below 19°C to ductile fracture with fibril formation and large-scale plasticity over 30°C.[16] These have revealed that the fracture mechanism of PTFE is rather sensitive to the temperature and the crystalline phases. Fibril formation leads to a pronounced change in the internal microstructure of PTFE before the FCP stage, especially in a high cycle fatigue (N_f) test. Therefore, FCI aspects in high N_f were investigated in detail in this study.

In the case of thermoplastic materials, cyclic creep aspects were found to be very significant in uniaxial tension–tension fatigue

Table I. Material Properties of PTFE

Density (kg/m^3)	DSC crystallinity (%)	T_g (°C)	Heat dissipation coefficient
2124.5 ± 0.1	51 ± 0.5	134	0.94

DSC, differential scanning calorimetry; T_g, glass-transition temperature.

tests because of temperature accumulation and stiffness reduction.[17] On the basis of the cyclic creep mechanism and microstructure features, the fatigue damage was found to mainly consist of three stages: the onset of coalescence, the propagation of matrix microcracks, and interface debonding and fiber breakage.[18] To numerically describe this failure process, a fatigue damage model was proposed by Nouri et al.[19] in the open literature. However, the formulation seems too complicated in experimental analysis. In this study, we intended to develop a simple and reliable phenomenological model for pure PTFE fatigue damage based on macroscopic observation.

Finally, the effects of the crystalline phases on the fatigue behavior of PTFE were experimentally studied and analyzed from different views with various equipment. The traditional fatigue data, including the stress–number of cycles to failure (S–N) curve and cyclic creep curves, were obtained. According to the continuous reduction of the gage area on the transverse section with increasing cycle number (N) until final fracture occurred, a phenomenological damage index (D) was defined to describe the fatigue damage of the PTFE samples. The fiber formation, orientation, and distribution on the fracture surfaces of the fatigued samples were observed by the scanning electronic machine. A microfocus hard X-ray diffraction (MH-XRD) beamline with a high spatial resolution supported by Shanghai Synchrotron Radiation Facility (SSRF) provided new insights to the mechanism of fatigue crack growth through the investigation of the crystallinity and lateral crystalline size on the fracture surface.

EXPERIMENTAL

Materials and Specimens

Investigations and examinations were carried out on PTFE, which is also known as Teflon. Table I shows the degree of crystallinity and other material properties of the pure PTFE powders, which were used to produce the fatigue samples with sintering and pressing treatments according to ASTM D 4894-98a. For thermoplastic materials, cyclic creep and large-scale plasticity generally occur in fatigue testing under a load control and lead to a very high level of strain amplitude and even subject the fatigue specimen to the risk of bucking. To prevent this, circular-shaped laminates with variable cross sections instead of traditional dog-bone-shaped samples were used to process the fatigue samples of PTFE with unified dimensions, as shown in Figure 1(A).

Test Procedure

Load-controlled tension–tension fatigue tests were performed on a Shimadzu MMT250 fatigue testing machine at ambient temperature in a range of cycles to failure from 0 to 10^7. Sinusoidal load cycles were applied with the load ratio kept at about zero (Load Ratio = Minimum load/Maximum load). The cyclic frequency was set to 5 Hz. The applied nominal stress was evaluated by the division of the applied load by the reference section area. For the PTFE material, about 20 specimens were tested with an imposed variable nominal initial stress before the fatigue test in the range from 10.00 to 13.36 MPa with a step of 0.42 MPa.

Strain in the axial loading direction was nonconnecting and was measured accurately with an advanced MMT250 machine. The maximum strain values were recorded at fixed time intervals during cyclic number accumulation, which allowed us to observe the cyclic creep and damage evolution. The crystalline phase transformation of PTFE material could be interpreted as the direct result of the temperature rise related to hysteresis and cyclic loading. Hence, the temperature on the surface of the specimen was continuously monitored during the whole fatigue test procedure by an NS9500 IR camera, as evidence of the crystalline phase distribution. To determine the influence mechanism of the crystalline phase transformation on the PTFE fatigue behavior with a microperspective, the fatigue fracture surfaces were observed with scanning electron microscopy. Extra information on the fracture surface was collected from new insight by MH-XRD, including the crystallinity and lateral crystalline size.

RESULTS AND DISCUSSION

Fatigue S–N Curves

Figure 2 shows the two categories of PTFE samples tested to failure. Compared with the samples without the fatigue test, PTFE showed better resistance to localized necking, and the two broadsides remained straight. The deformed region undertook the most plasticity and got into the large deformation research level with an axial strain obviously over 5%.

The fatigue life curves (S–N) for the PTFE samples are reported in Figure 3, in which the initial nominal stress is plotted via the number of cycles to failure. The S–N curve of the pure PTFE material consisted of two zones: period I, where a steep drop in the applied stress occurred up to 10^5 cycles, and period II, where the curve was almost horizontal up to 10^7 cycles. According to reports[20] that demonstrated that a fatigue life limit did not exist for metal materials, the fatigue samples finally

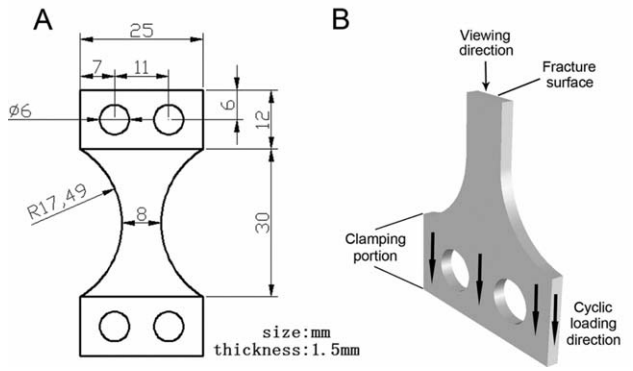

Figure 1. (A) Dimensions of the tested specimen. (B) Test conditions for the PTFE samples and the observation method for MH-XRD and scanning electron microscopy.

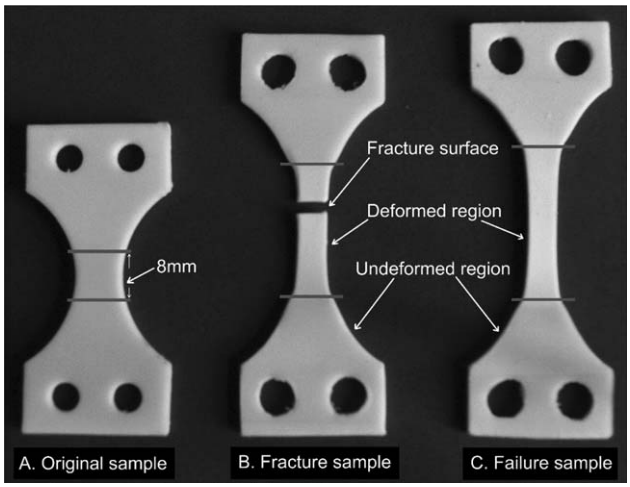

Figure 2. (A) Original sample without fatigue test and two different results of fatigue failure, (B) final fracture with an low initial stress (10.00–12.10 MPa), and (C) softening failure with high initial stress (12.52–13.36 MPa). The axial initial test length of the deformed region was 8 mm (S_{max} = maximum nominal stress).

fractured with large possibility when N accumulated beyond 10^7 with a consideration the lower power of van der Waal's forces compared to those of interatomic forces in the metal materials and the semicrystalline nature of the PTFE material. We devote ourselves to confirming the stepwise type[21] of the S–N curve of the PTFE material in a future study.

The test results included run-out points after 10^7 cycles and partial data tested at a frequency of less than 5 Hz with square marks by contrast to that tested under the same stress level with a frequency of 5 Hz and failure by bucking due to excessive heating and softening. Slowing down the loading frequency improved the fatigue performance of PTFE to some extent. However, the limited extent showed no significant influence on the trend of the S–N curve.

Cyclic Creep and Fatigue Damage

We evaluated the cyclic creep aspects during the fatigue test by plotting the strain in the deformed region measured by MMT250 versus N, as shown in Figure 4. According to the fatigue life, the strain curves could be considered:

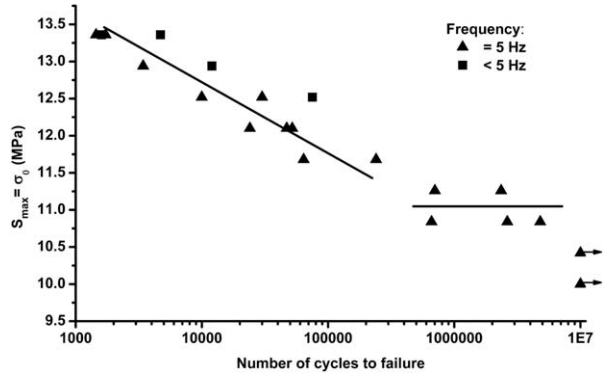

Figure 3. S–N curve of PTFE: (▲) whole stress level at 5 Hz and (■) higher stress level at a lower frequency (1 Hz for 13.36 MPa and 2 Hz for 12.94 and 12.52 MPa).

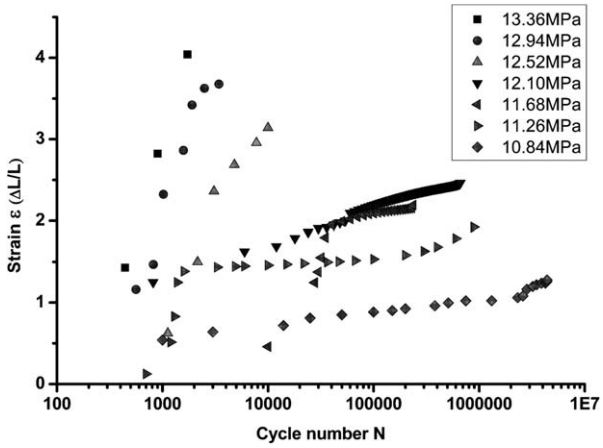

Figure 4. Strain elongation with loading cycle accumulation under various initial stresses (13.36–10.84 MPa). ΔL is the elongation of the axial length in the deformed region. The frequency was 5 Hz.

1. In low N_f ($N_f < 10^5$), where a J or line pattern in the strain occurred until final failure without an obvious FCI stage; this was similar to the finding reported by Andrews and Walker[22] in an unnotched polyethylene fatigue test.
2. In high N_f ($10^5 < N_f < 10^7$), where the rate of strain accumulation tended to stabilize for a long period at lower stress after a short but steep rising stage. During the approach to failure, the increase in the strain was reproduced because to the onset of FCP. Additionally, the more the stress decreased, the more portion of fatigue life the FCI stage consumed, including the short rising and stabilization stages: 67.5% at 11.25 MPa and 88.6% at 10.83 MPa. With the progressive decrease in stress, the portion presumably took over 90%, such as in the very high-N_f result for metal materials.[23]

As Figure 2 shows, the gage area vertical to the loading direction kept a uniformed reduction during the cyclic creep process in the deformed region. Hence, the fatigue damage could simply be described as a reduction in the gage area according to the cyclic number at a macroscopic level. In these large-strain experiments, an assumption of constant volume[7] in the deformed region, which was proven to be true for strains greater than approximately 5%, was used to calculate D, defined in this work as follows:

$$D = 1 - \frac{A}{A_0}$$

where A_0 is the area of the minimum cross section in deformed region of original samples, $A_0 = 8\ \text{mm} \times 1.5\ \text{mm}$, A is the gage area in real time, proposed as the volume (V) dividing the uniaxial length $L = (1 + \varepsilon)L_0$ in the deformed region (where ε is the strain and L_0 is its original length). The evolution of D is represented for the PTFE material in Figure 5 as a function of N. Two typical damage curves for low and high N_f are indicated, and the damage evolution occurred according to three stages, which conformed to the model proposed by Nouri et al.[19] for composite material fatigue. Stage 1 corresponded to the onset of crack initiation, which contained the transformation of the crystalline and internal structure of PTFE and matrix

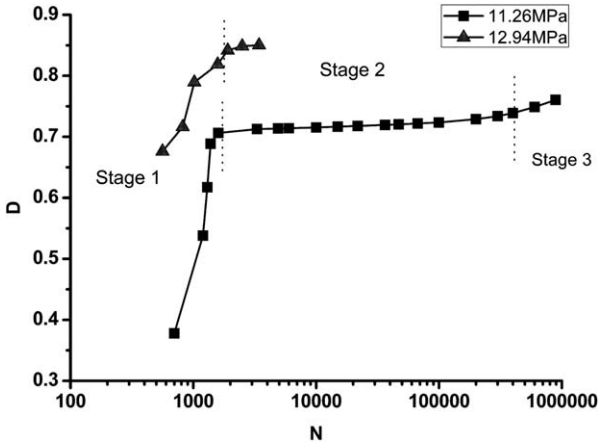

Figure 5. *D* versus *N*.

microvoids. The higher levels of imposed load were, the higher extent of the damage was, and hence, *N* was lower for stage II, which corresponded to the coalescence and propagation of the microdiscontinuities created during stage 1. The fibrosis and microvoids promoted balance between the thermal energy accumulation and dissipation. The temporary moderation of stiffness reduction of PTFE was observed in stage 2 before stage 3. The last stage exhibited macroscopic crack propagation with fiber fracture and interlayer stripping, which resulted in a rapid stiffness reduction until final fracture occurred.

Crystalline Phase Transformation

The aspects of crystalline phase transformation during fatigue testing under load control were observed and analyzed by various precision machines, including an NS9500 IR camera, a scanning electronic machine, and a microfocus hard X-ray beam line (BL15U1) supported by SSRF.

Thermal Distribution on Fatigue Samples. During the fatigue test, the IR camera was used to record the thermal field of the deformed region of the fatigue samples. Figure 6 shows the general process of temperature variation in the fatigue test. The thermal field expanded hierarchically with local softening and increasing axial strain; this indicated the sufficiency of the MMT250 system for the PTFE fatigue test. As discussed at length by Rae and Brown[8] for PTFE tensile tests, PTFE showed two crystalline transitions at atmospheric pressure: at 19°C from the triclinic structure (phase II) to a partially ordered hexagonal structure (phase IV) with an unraveling in the helical conformation and then at 30°C to a pseudohexagonal structure (phase I) with further rotational disordering and an untwisting of the helices. Hence, the temperature was the main reason for the phase transformation. The deforming process could be described in turn as energy accumulation under cyclic loading, increasing temperature, phase transformation, helices orientation along the uniaxial loading direction, and finally, increasing strain.

According to the energy theory, this microstructure transformation would be beneficial for internal energy absorption and dissipation, and fatigue crack also was initiated due to the increase in temperature and structural reengineering; this was in agreement with previous studies.[24,25] To analyze the phase distribution in the fatigue fracture region, the temperature field on the cross section (A–B in Figure 6) located the maximum temperature (T_{max}) was mapped, as shown in Figure 7. The difference in the phase pattern was observed between the edge of the A–B cross section and the center of the FCI region. The phase I and IV crystalline structures mainly occurred in the PTFE material during the fatigue test, as shown in Figure 7. Phase I appeared on the whole fracture section of the low-N_f sample under high stresses (11.68–13.36 MPa), whereas it was concentrated in the FCI region of high-N_f samples under lower stresses (11.26 and 10.84 MPa). This imparted the phase IV structure to the FCP region. The dissipation effect of phase transformation was proven to be effective for the stabilization of strain and temperature in high N_f from Figure 4. However, in the low-N_f process, the chain straightening in the phase I structure of the PTFE material under a high temperature and strain rate accelerated

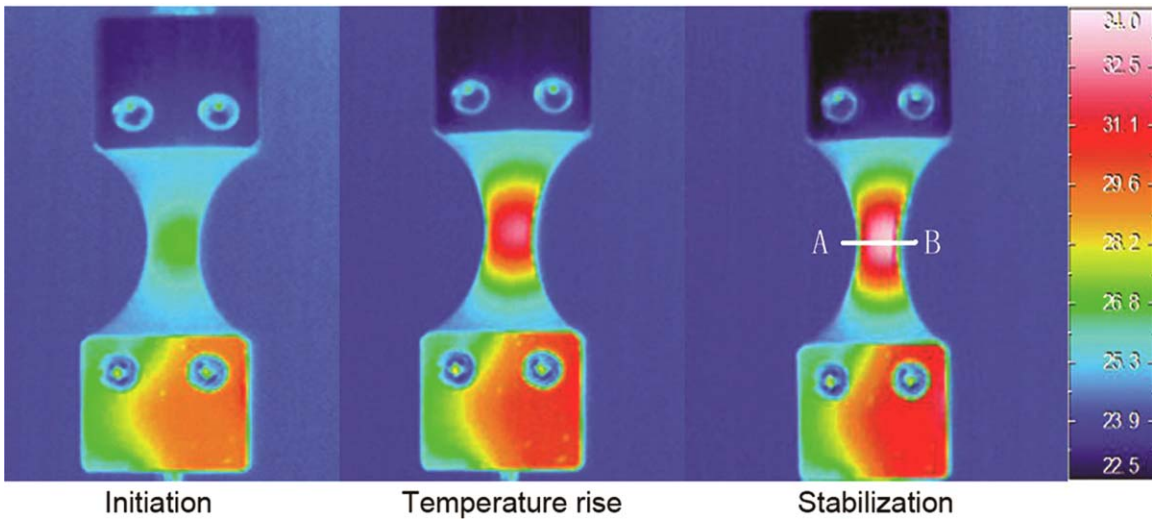

Figure 6. General process of increasing temperature of the PTFE samples with conditions of 10.84 MPa and 5 Hz, sections A and B represent the location of T_{max} during the stabilization period. [Color figure can be viewed in the online issue, which is available at wileyonlinelibrary.com.]

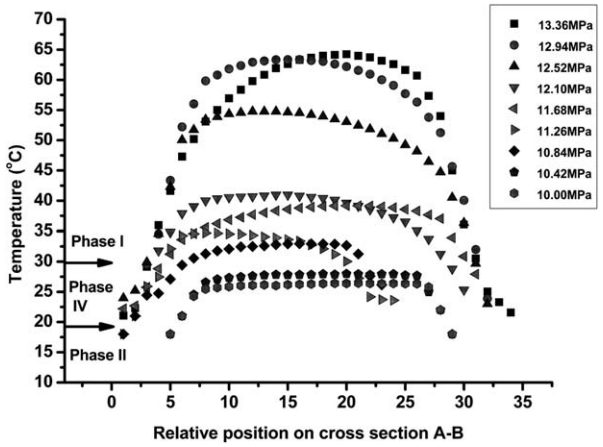

Figure 7. Temperature distribution on the A–B lines of the PTFE specimen surfaces shown in Figure 6

the nucleation and growth of new stress-induced structural defects that did not exist in the initial nondeformed configuration until final fracture.

The chain straightening in the phase I structure was also found to be beneficial for the enhancement of the tensile strength during cyclic creep. Figure 8 shows the changes in temperature and tensile stress according to the variations of initial stresses. From 10.00 to 13.36 MPa, the phase I structure of PTFE started to appear and expanded to the scope, and the corresponding true failure stresses increased more than double, from 23.75 to 58.22 MPa. The T_{max} curve in Figure 8 presents an increasing type of double line, with a transition point at 40°C. Over 40°C, the T_{max} showed a rapid increase, and the PTFE material was subject to a challenge of cyclic loading. This was probably related to the intensified friction and softening caused by a wide range of fibrosis under high stresses.

Microstructure on the Fracture Surface. Rae, Brown, and coworkers[7,8,16] discussed, PTFE material presents different crystalline phase structures under different temperature conditions. Under the inducement of uniaxial loading, these microstructures in various crystalline phases form different macromorphologies, which are easy to distinguish by scanning electronic microscopy. For example, the fiber can be found on the fracture surface of the tensile test sample at a temperature over 30°C, when the crystalline structure is in phase I. Thus, the effects of the phase transformation on the fatigue fracture of the PTFE material can be intuitively understood through analysis of the evolved fracture morphology and temperature conditions.

Figure 9 shows an overview of the fracture surfaces after the fatigue test under various stress levels. According to the curves of the temperature distribution shown in Figure 7, the temperature in the FCI region was over 30°C, and PTFE in phase I exhibited substantial fiber formation. The fibrosis level in the FCI region increased with the initial stresses, with laminar fibers at high stress levels [Figure 9(A,B)] but stringlike fibers at low stress levels [Figure 9(C,D)]. The fibrosis level also affected the fracture pattern in the FCP region. At a stress level of 13.36 MPa, the crack propagation paths presented bumpiness, and even some fibrous layers were peeled off. However, at a stress level of 10.84 MPa, the overall paths were flatter, and the fracture surface appeared to be well-bedded from the FCI region to the FCP region. Figure 10 represents the different morphologies between the FCI and FCP regions on the fracture surface at 10.84 MPa and 5 Hz. The crystalline phase of PTFE in the FCI region was in phase I, and the region exhibited substantial fiber formation [Figure 10(A,B)] and a network of fibrils [Figure 10(C)]. However, the crystalline phase turned into phase IV with decreasing temperature below 30°C in the propagation region, as compared with Figure 7. The amount of plastic deformation and dimple structure found in the FCP region are shown in Figure 10(D).

Under higher magnification, the processes of fiber formation and orientation were observed, as shown in Figure 11. The crystalline phase of the PTFE material converted into phase I in the FCI region from phase IV in the FCP region, as shown in Figure 11(A). Some short fibers [Figure 11(C)] dispersed in the transitory region, which was evidence of original fiber formation. Closer to the crack source, the fibers were longer and more assembled, and they oriented along the fracture direction. Hence, a reasonable process of FCI for the PTFE materials was proposed. A local temperature rise led to the crystalline phase transformation, and fibers were formed with molecular untwisting. Microvoids and stress concentration caused by multiplied fibrosis promoted the onset of microcracks. Finally, the fiber orientation helped the continuous microcracking until a main crack formed. This conclusion implied that the crystalline phase transformation had a pronounced effect on the FCI mechanism of the PTFE material, and local fibrosis was the main reason for FCI. Meanwhile, these observations on fiber formation and orientation also provided a reliable interpretation for the enhancement of the tensile strength and stiffness with increasing temperature and stress, as shown in Figure 8.

Crystalline and Lateral Crystallite Size. The MH-XRD beamline was used for the investigation of cyclic-load-induced crystallization. The MH-XRD had a high intensity, high luminance, high stability, and high temporal and spatial resolution. It was found to be a powerful tool for detecting the strain-induced

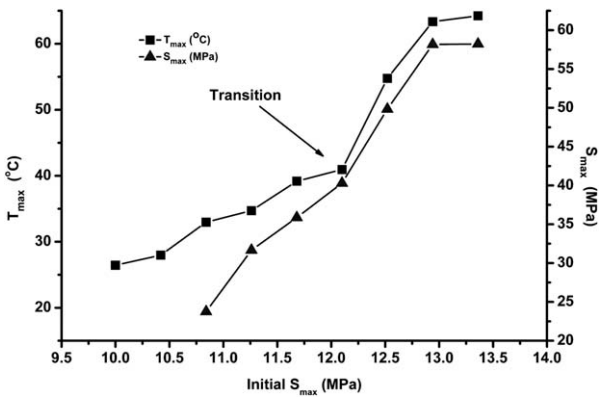

Figure 8. T_{max} and maximum true stress (S_{max}) according to the variation of the initial stress, T_{max} for the highest temperature values of each curve in Figure 7, and S_{max} for the corresponding true stresses.

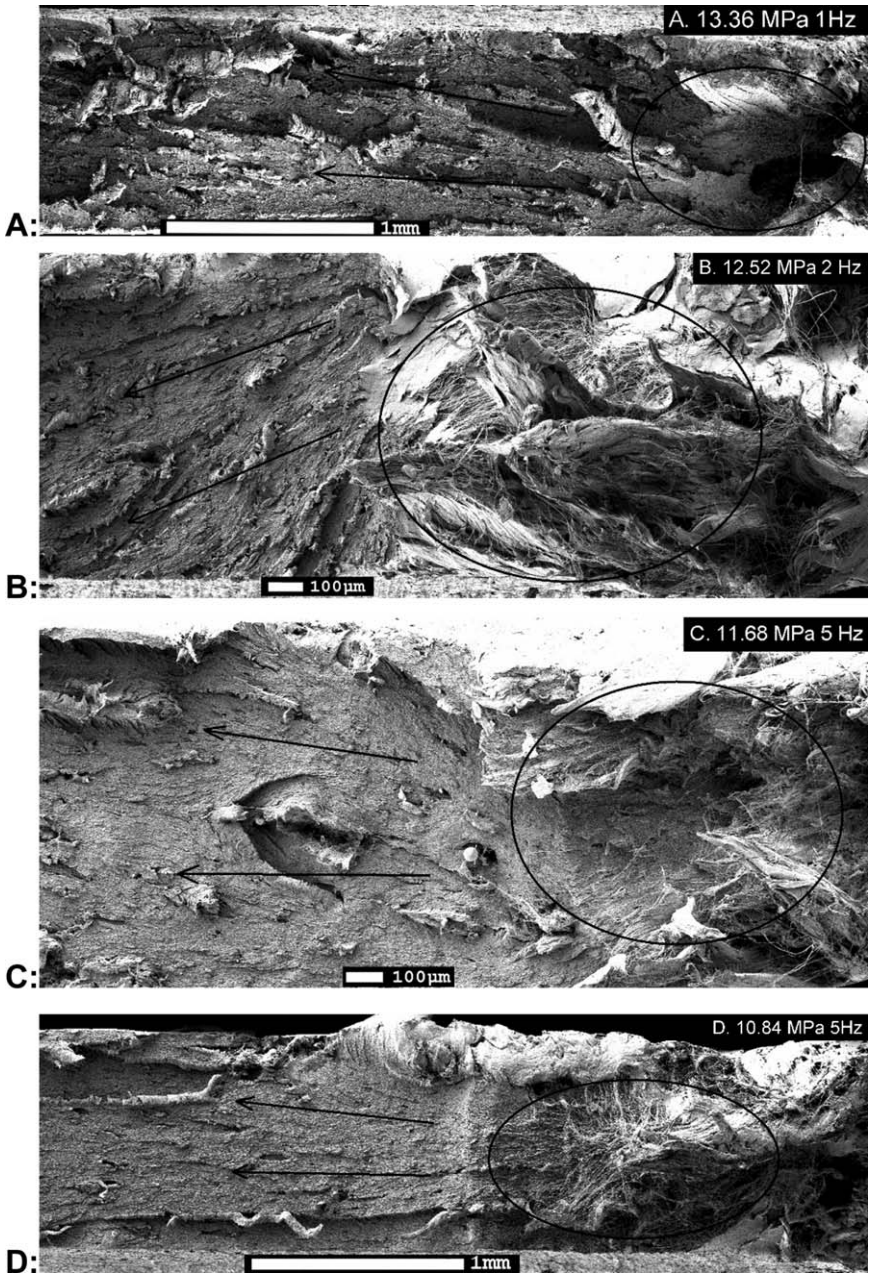

Figure 9. Overviews of the fracture surfaces in low and high N_f, where the black boundaries indicate the crack initiation regions and the black arrows indicate the failure propagation paths.

crystallization of microdomains.[26] However, in the limited service time provided by SSRF, only one high-N_f sample (Figure 10) was detected by MH-XRD. To characterize the crystallization induced by cyclic loading, the diffraction patterns were recorded by the scanning of the fracture surface on the x axis along the crack propagation direction. The center of the short edge near the FCI region was taken as the origin of coordinates. Each displacement was 1 mm. For comparison purposes, the corresponding diffraction patterns of the original sample before the fatigue test were also observed, as shown in Figure 12. A slightly oriented diffraction and a large increase in the crystallinity was observed in a comparison of the two patterns before and after the fatigue test.

For more clarity, the crystallinity and lateral crystallite size were calculated according to the diffraction patterns shown in Figure 11(A,B). The crystallinity (X_c) was calculated from the resulting Gaussian peak as follows:

$$X_c = A_c / A_c + A_a$$

where A_c and A_a represent the integrated intensities of the crystalline and amorphous regions, respectively. The crystalline size was estimated with the Scherrer equation:

$$L_{100} = \frac{k\lambda}{\beta_{100}} \cos\theta$$

where L_{100} is the crystallite size in the direction perpendicular to the (100) plane, $\lambda = 0.124$ nm is the wavelength, and $\theta = 9.05°$ is

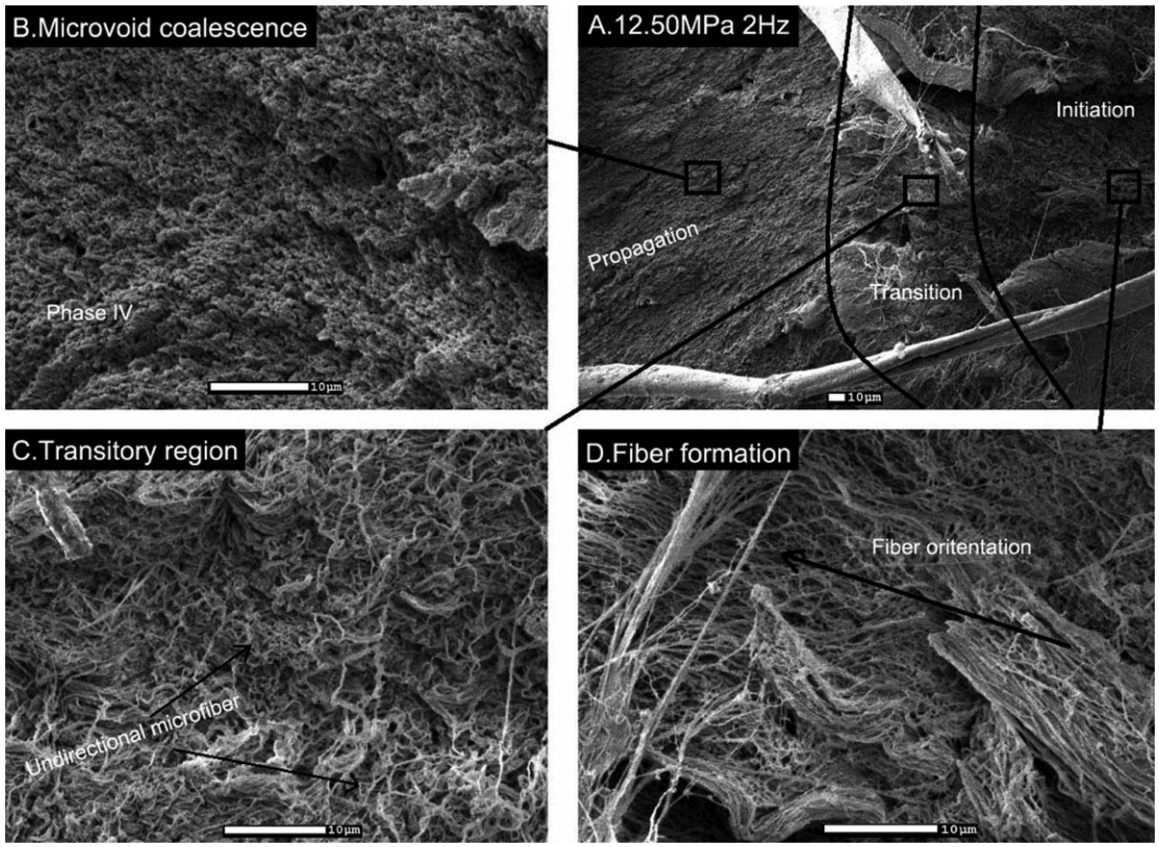

Figure 10. Fracture surface of the PTFE sample at 10.84 MPa and 5 Hz.

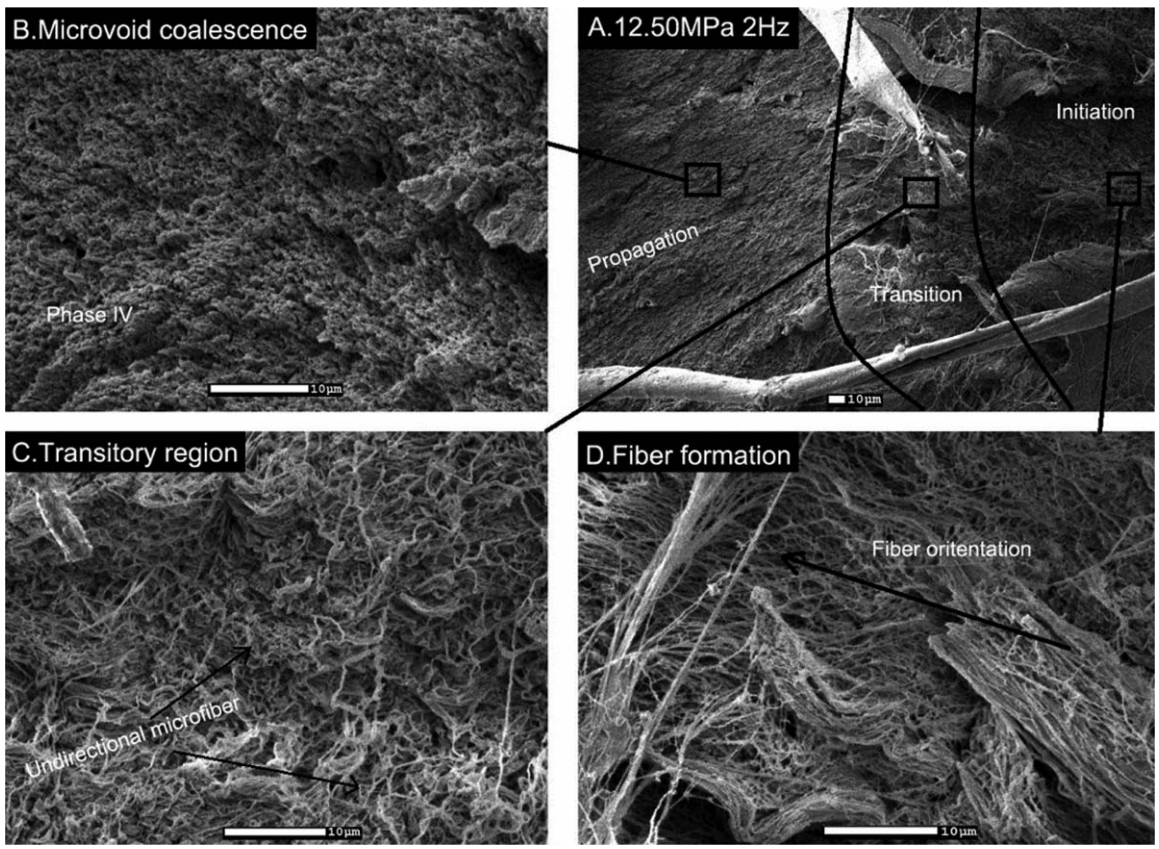

Figure 11. Transitory region of the PTFE fatigue sample at 12.5 MPa and 2 Hz.

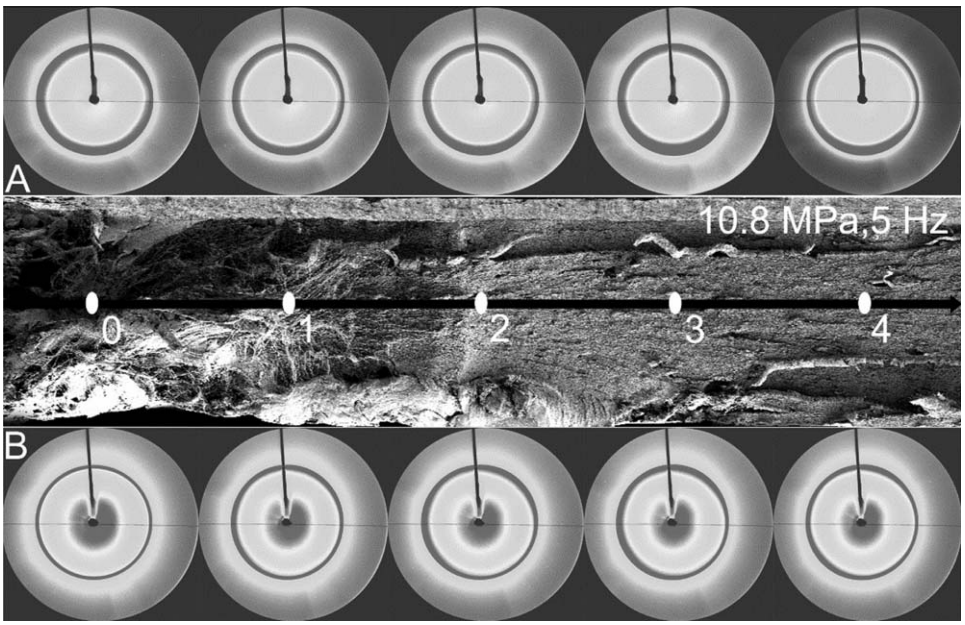

Figure 12. Two-dimensional XRD patterns distributed along the fracture direction, the white dots indicate the observation positions on the A and B surfaces, A is the original sample without the fatigue test, and B is the tested sample at 10.84 MPa and 5 Hz.

the Bragg angle. The Scherrer factor (k) is 0.89, and β_{100} is the half-width of the (100) reflection in the radial direction.[27]

After the fatigue test, the crystallinity increased over 70% from 51%; in particular, it was 77% at the initial crack center, and the PTFE material had almost a 1.5 times smaller later crystallite size than the original sample. These both indicated a pronounced effect of the prevention of crack growth and induced crack bifurcation.[28,29] Meanwhile, the highest crystallinity and smallest lateral crystallite size appeared at the initial center, and the levels decreased far away from the center. The reason was that the crystalline structure of PTFE in phase I supported more motivation for the chains interacting into nucleation with cyclic-load inducement. The MF-XRD experimental data exposed the effect of the crystalline phase transition on the PTFE fatigue behavior, which was a new insight.

CONCLUSIONS

In summary, the low- and high-N_f tests of unnotched samples made of pure PTFE were performed to investigate the effect of the crystalline phase transformation on the FCI and fracture mechanism of the PTFE materials. The FCI stage was found to take up most of the fatigue life, 88.6% at 10.84 MPa, in the high-N_f test ($10^5 < N_f < 10^7$). A simple phenomenological damage model was defined to describe the cyclic creep process, and the result was satisfying. Additionally, the strong effect of crystalline phase transformation on the FCI and fracture mechanism of PTFE materials was revealed by different means. The local fibrosis in the phase I structure of PTFE was proven to be the onset of FCI. The crystalline structure in phase I in the FCI region with a higher crystallinity and smaller crystalline size showed a greater effect of preventing the crack growth compared to that in phase IV in the FCP region.

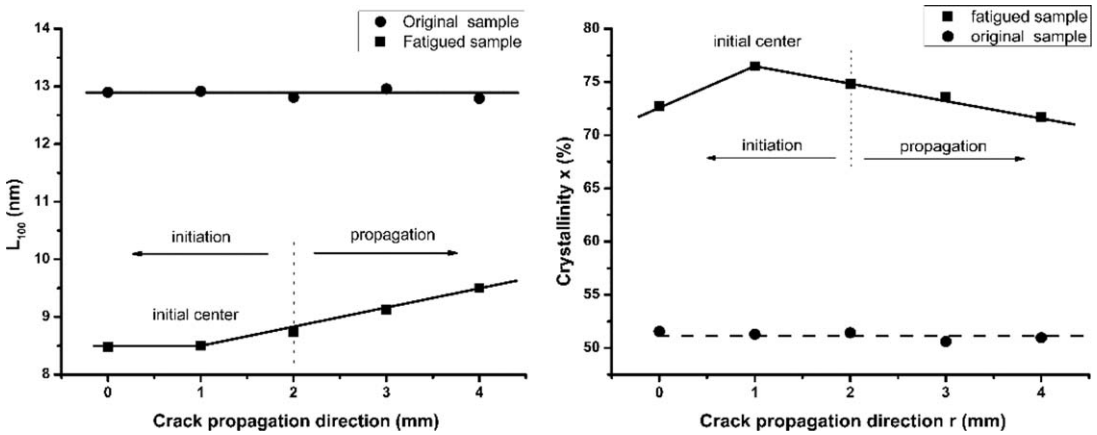

Figure 13. Crystallinity and lateral crystalline size corresponding to Figure 12.

ACKNOWLEDGMENTS

The microfocus X-ray beam line (BL15U1) was supported by SSRF. This work was financially supported by Chinese National Science Foundation (contract grant numbers 11327801 and 11172188). The authors acknowledge the support of Chao He, Muhammad Kashif, and Guoxia Fei.

REFERENCES

1. Leibner, E. S. Jet Blown PTFE for Control of Biocompatibility; The Pennsylvania State University, UMI Dissertations Publishing: **2009**; p 21.
2. Sperati, C. A.; Starkweather, H. W., Jr. *Adv. Polym. Sci.* **1961**, *465*, 95.
3. Cox, J. M.; Wright, B. A.; Wright, W. W. *J. Appl. Polym. Sci.* **1964**, *8*, 2935.
4. Xiang, D.; Tao, K. *J. Appl. Polym. Sci.* **2007**, *103*, 1035.
5. Briscoe, B. J.; Ni, Z. *Wear* **1984**, *100*, 221.
6. Sauer, J. A.; Richarason, G. C. *Int. J. Fracture* **1980**, *16*, 499.
7. Rae, P.; Dattelbaum, D. *Polymer.* **2004**, *45*, 7615.
8. Rae, P. J.; Brown, E. N. *Polymer* **2005**, *46*, 8128.
9. Righetti, M. R.; Boggioni, A.; Laus, M.; Antonioli, D.; Sparnacci, K.; Boarino, L. *J. Appl. Polym. Sci.* **2013**, *130*, 3624.
10. Faughnan, P.; Bryan, C. *J. Mater. Sci. Lett.* **1998**, *17*, 1743.
11. Zhang, Z.; Aglan, H.; Faughnan, P.; Bryan, C. *J. Reinf. Plast. Compos.* **1998**, *17*, 752.
12. Avanzini, A.; Donzella, G.; Gallina, D.; Pandini, S.; Petrogalli, C. *Compos. B.* **2013**, *45*, 397.
13. Gan, Y. X.; Aglan, H.; Faughnan, P.; Bryan, C. *J. Reinf. Plast. Compos.* **2001**, *20*, 766.
14. Friedrich, K.; Walter, R.; Voss, H.; Karger-Kocsis, J. *Composites* **1986**, *17*, 205.
15. Bunn, C. W.; Howells, E. R. *Nature.* **1954**, *4429*, 549.
16. Brown, E. N.; Rae, P. J.; Orler, E. B.; Gray, G. T., III.; Dattelbaum, D. N. *Mater. Sci. Eng. C.* **2006**, *26*, 1338.
17. Avanzini, A.; Donzella, G.; Gallina, D.; Pandini, S.; Petrogalli, C. *Compos. B.* **2013**, *45*, 397.
18. Toubal, L.; Karama, M.; Lorrain, B. *Int. J. Fatigue* **2006**, *28*, 1867.
19. Nouri, H.; Meraghni, F.; Lory, P. *Int. J. Fatigue* **2009**, *31*, 934.
20. Bathias, C. *Fatigue Fract. Eng. Mater. Struct.* **1999**, *22*, 559.
21. Shiozawaa, K.; Hasegawa, T.; Kashiwagi, Y.; Luc, L. *Int. J. Fatigue* **2009**, *31*, 880.
22. Andrews, E. H.; Walker, B. *J. Proc. R. Soc. Lond. A* **1971**, *325*, 57.
23. Wang, Q. Y.; Berard, J. Y.; Rathery, S.; Bathias, C. *Fatigue Fract. Eng. Mater. Struct.* **1999**, *22*, 673.
24. Huang, Z. Y.; Wagner, D.; Wang, Q. Y.; Bathias, C. *Mater. Sci. Eng. A* **2013**, *559*, 790.
25. Wang, Q. Y.; Lib, T.; Zenga, X. G. *Proc. Eng.* **2010**, *2*, 65.
26. Yan, N.; Xia, H.; Zhan, Y.; Fei, G. *Macromol. Mater. Eng.* **2013**, *298*, 38.
27. Klug, H. P.; Alexander, L. E. In X-Ray Diffraction Procedures for Polycrystalline and Amorphous Materials, 2nd ed.; Wiley-Interscience: New York, **1974**; p 687.
28. Beurrot, S.; Huneau, B.; Verron, E. *J. Appl. Polym. Sci.* **2010**, *117*, 1260.
29. Saintier, N.; Cailletaud, G.; Piques, R. *Mater. Sci. Eng. A* **2011**, *528*, 1078.